Computational electrocatalysis: methods and fundamental applications on CO2 reduction and formic acid oxidation

Granda Marulanda, L.P.

Sagrada Família
Barcelona, Catalonia, Spain

4 A SEMIEMPIRICAL METHOD TO DETECT AND CORRECT DFT-BASED GAS-PHASE ERRORS AND ITS APPLICATION IN ELECTROCATALYSIS

Computational models of adsorption at metal surfaces are often based on DFT and make use of the generalized gradient approximation. This likely implies the presence of sizable errors in the gas-phase energetics. Here, we take a step closer toward chemical accuracy with a semiempirical method to correct the gas-phase energetics of PBE, PW91, RPBE, and BEEF-vdW exchange–correlation functionals. The proposed two-step method is tested on a data set of 27 gas-phase molecules belonging to the carbon cycle: first, the errors are pinpointed based on formation energies, and second, the respective corrections are sequentially applied to ensure the progressive lowering of the data set's mean and maximum errors. We illustrate the benefits of the method in electrocatalysis by a substantial improvement of the calculated equilibrium and onset potentials for CO_2 reduction to CO on Au, Ag, and Cu electrodes. This suggests that fast and systematic gas-phase corrections can be devised to augment the predictive power of computational catalysis models.

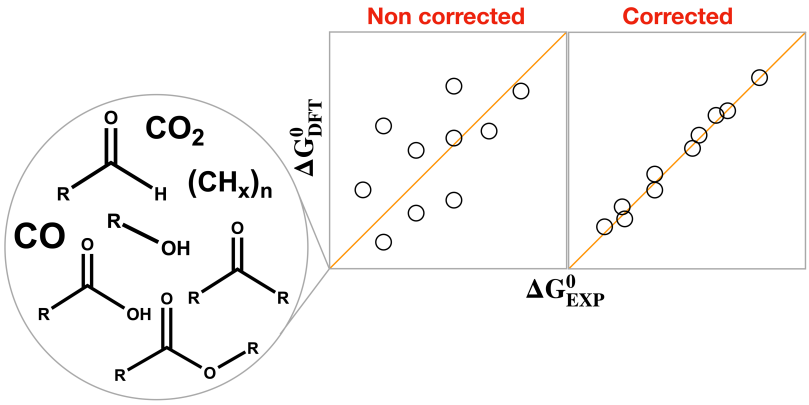

This chapter is based on Granda-Marulanda, L. P.; Rendón-Calle, A.; Builes, S.; Illas, F.; Koper, M. T. M.; Calle-Vallejo, F. A Semiempirical Method to Detect and Correct DFT-Based Gas-Phase Errors and Its Application in Electrocatalysis. ACS Catal. 2020, 10 (12), 6900–6907

4.1 Introduction

For decades, considerable effort has been devoted to increasing the accuracy of density functional theory (DFT). This has been done by developing more accurate exchange-correlation functionals at the generalized gradient approximation (GGA) level,[1–3] hybrid functionals,[4–6] and range-separated functionals.[7–9] In addition, different correction schemes have been developed to account for electron localization[10] or dispersion interactions.[11–13] Lately, machine learning schemes[14] have also been proposed to bypass Kohn-Sham equations. In general, these efforts include careful computational benchmarking and comparison to experiments.[15–17]

An agreement has been reached in the scientific community about the level of theory required to simulate certain materials with a good tradeoff between computational time and accuracy. For instance, hybrid functionals are advisable for molecules and solids with localized electrons, while GGAs usually suffice for bulk and surface metals.[13,16] However, the choice is not trivial when dealing with systems where metals and molecules are involved and ought to be simulated at the same level of theory. In such a case, the accuracy may be improved by using GGA functionals and adding semiempirical corrections to the DFT energies of molecules, as done for thermochemical reaction energies of interest in catalysis,[18,19] formation and decomposition energies of solids,[20,21] and catalytic kinetic barriers.[22,23]

In this ***Chapter***, we provide a simple and fast procedure for detecting gas-phase errors based on the formation energies of reactants and products calculated with DFT. Improving the description of the gas-phase is shown to enhance catalytic predictive power by analyzing the electrocatalytic CO_2 reduction reaction to CO on Au, Ag, and Cu electrodes. The reduction of CO_2 and CO (hereafter denoted as CO_2RR and CORR, respectively) are of great importance in catalysis science and technology, as they lead to valuable feedstocks and fuels such as methane, ethylene, ethanol, and formic acid while helping in balancing the carbon cycle.[24–26] Although DFT has been used to predict enhanced catalysts for other electrocatalytic reactions,[27–29] it has been so far challenging to elaborate robust design routines for CO_2RR and CORR to hydrocarbons and oxygenates.[30] Thus, the method presented in this ***Chapter*** may help boost materials design via screening for those paramount reactions.

4.2 Computational Methods

All calculations were performed using the Vienna Ab initio Simulation Package.[31] Dissimilar gas-phase errors have been pointed out in previous studies for the total energy of CO(g) and CO_2(g)[18,19,32] using PBE and RPBE.[33] In addition, others suggested a correction for the total energy of H_2(g) to be applied only when using BEEF-vdW.[34] Thus, we made a functional-dependent analysis including four different xc functionals habitually used in catalysis, namely PBE,[35] PW91,[36] RPBE,[33] and BEEF-vdW.[9]

The gas-phase molecules were relaxed with the conjugate gradient algorithm in boxes of ~3375 Å^3, considering only the Γ point. The effect of the cores on the valence electron density are incorporated using the projector-augmented wave

(PAW) method.[37] To compute the formation energies of the molecules, graphite was represented by graphene. Approximating graphene as the standard state of carbon is based on the weak interlayer cohesive energy of graphite (0.031 - 0.064 eV/atom)[38–43] (see Section C6 in Appendix C). The optimized interatomic distances of graphene are 1.43 (PBE and RPBE) and 1.42 Å (PW91 and BEEF-vdW).

The convergence criterion for the maximal forces on the atoms for all simulations was 0.01 eV $Å^{-1}$, and the plane wave cutoff was set to 400 eV. Convergence tests for the free energy of reaction of $CO_2(g) + H_2(g) \rightarrow CO(g) + H_2O(g)$ with plane-wave cutoffs in the range of 300 – 1000 eV within PBE showed that 400 eV is enough to achieve accurate reaction energies with an average difference of ~5 meV (see Table C1). None of the species analyzed has unpaired electrons, so spin unrestricted calculations were not required. Gaussian smearing with $k_BT = 0.001$ eV was used. In all cases, the energies were extrapolated to 0 K.

The reaction free energies were obtained as $\Delta G^0 = \Delta E_{DFT} + \Delta ZPE - T\Delta S^0$, where ZPE is the zero-point energy contribution calculated from the vibrational frequencies obtained using the harmonic-oscillator approximation. The standard total entropies (S^0) and the experimental standard free energies (ΔG^0_{exp}) were obtained from thermodynamic tables[44–46] at T = 298.15 K. In cases where ΔG^0_{exp} was not tabulated, it was evaluated by combining entropy and enthalpy values: $\Delta G^0_{\text{exp}} = \Delta H^0_{\text{exp}} - T\Delta S^0_{\text{exp}}$. We did not include heat capacity effects as recent studies showed that formation energies are not significantly modified by them from 0 to 298.15 K.[21]

Electrocatalytic CO_2 reduction to CO was modeled based on the free energy scheme described in previous reports,[47] making use of the computational hydrogen electrode[48] for the description of proton-electron transfers. The reaction pathway proceeds via CO_2 hydrogenation (step 1: $CO_2 + H^+ + e^- + * \rightarrow *COOH$), followed by *CO formation (step 2: $*COOH + H^+ + e^- \rightarrow *CO + H_2O_{(l)}$), and desorption (step 3: $*CO \rightarrow * + CO$). In this approach, the onset potential is numerically equivalent to the additive inverse of the largest positive reaction energy considering steps 1 and 2 only ($U_{onset} = -\max(\Delta G_1, \Delta G_2)/e^-$) as step 3 is not electrochemical. We note that alternative pathways for CO_2RR to CO in the experimental literature suggest that CO_2 may be activated by an electron transfer prior to its adsorption, and the adsorbed species is stabilized by a hydrated cation close to the surface.[49–53] Since the modeling of decoupled proton-electron transfers is challenging from a plane-wave DFT standpoint, here we limit ourselves to the standard mechanism[47] using corrected gas-phase energies.

4.3 Results and Discussion

4.3.1 Pinpointing Errors

The data set used to determine the errors (data set A) consists of 27 molecules involved in the CO_2RR and CORR, in which we include at least one representative molecule of the following functional groups: hydrocarbons, alcohols, carboxylic acids, esters, ethers, aldehydes, and ketones. We included

compounds with one to five carbon atoms in the structure (see the full list of compounds in Table C2). Data set A contains the DFT-calculated standard free energy of formation (ΔG^0_{DFT}) of the target molecules (γ) using C(s), O_2(g), and H_2(g) as a reference:

$$aC + bO_2 + cH_2 \rightarrow \gamma \qquad 4.1$$

For instance, for acetaldehyde, Eq. 4.1 is $2C + \frac{1}{2}O_2 + 2H_2 \rightarrow C_2H_4O$. The total errors in the formation energy of each molecule in data set A (ε_T), represent the discrepancy between ΔG^0_{DFT} and ΔG^0_{exp}:

$$\varepsilon_T = \Delta G^0_{DFT} - \Delta G^0_{\text{exp}} \qquad 4.2$$

It is worth noting that ε_T can either be positive or negative (or zero, in case there is a perfect energetic description). As a first approximation, we consider a group-additivity type of scheme[54] where a given molecule with different functional groups may have different errors present in its ΔG^0_{DFT}. Thus, the total error (ε_T) can be decoupled in the separate contributions of the functional groups present in the molecule (ε_i). In mathematical terms this is expressed as: $\varepsilon_T \approx \sum_{i=1}^{n} \varepsilon_i$, so that the total error with respect to experiments for a given molecule (ε_T) is approximately the sum of the errors inherited from the *n* functional groups present in the molecule (ε_i). As shown in Table C2, data set A is formed by CO, CO_2, and molecules containing CH_x, hydroxyl, carbonyl, carboxyl, ether, and ester functional groups.

A second data set (data set B) consists of calculated free energies of reaction for the CO_2RR and CORR to produce the molecules in data set A (see Tables C3-C4). We use data set B to verify whether the corrections implemented in data set A are appropriate. This is the case when there is a decrease in the mean absolute error (MAE) and maximum absolute error (MAX) in data set B as the corrections are successively applied. The free energies of reaction in data set B are grouped in two: firstly, reactions with CO as a reactant and γ as a product, as shown in Eq. 4.3 (see Table C4).

$$gCO + kH_2 \rightarrow \gamma + mH_2O \qquad 4.3$$

For instance, for acetaldehyde, Eq. 4.3 is: $2CO + 3H_2 \rightarrow C_2H_4O$. Particular cases are the formation of CO_2 and HCOOH from CO, which follow Eq. 4.4.

$$CO + H_2O \rightarrow \gamma + rH_2 \qquad 4.4$$

Secondly, data set B contains reactions with CO_2 as a reactant and γ as a product, as shown in Eq. 4.5 (see Table C3).

$$xCO_2 + yH_2 \rightarrow \gamma + zH_2O \qquad 4.5$$

Eq. 4.5 applied to acetaldehyde is: $2CO_2 + 5H_2 \rightarrow C_2H_4O + 3H_2O$. In these equations, water is considered to be in gas phase ($H_2O(g)$; see Section C3 in the Appendix C). We categorized the errors for each functional based on organic functional groups (-CH_x, hydroxyl, carbonyl, carboxyl, ether, and ester functional groups) and molecules (in particular, CO and CO_2), as shown in Table 4.1. For example, acetaldehyde has one -CH_x (-CH_3) group and one carbonyl (-CHO) group. Table C5 contains the corrections added per exchange-correlation functional and organic functional group.

The errors in the standard free energies (hereafter referred to simply as errors) in Table 4.1 are xc-functional-dependent, so that the signs and magnitude change in each case, in line with previous studies.[16] This dependence can be expected because exchange-correlation functionals are fitted for certain applications using different data sets.[9,55] In the following, we will explain how the errors in Table 4.1 were determined, taking PBE as an example. Note in passing that the analysis is similar for the other functionals included in this study, and all values are tabulated in Section C4 of the Appendix C.

To pinpoint the errors, we first determined all deviations (ε_T) in the calculated free energies of formation of the molecules in data set A relative to the experimental ones using Eq. 4.2. We paid special attention to CO_2 and CO as they are the reactants of CO_2RR and CORR, respectively (all reactions in data set B). For PBE, the error in CO_2 is $\varepsilon_T^{CO_2} = -0.19$ eV, whereas that of CO is $\varepsilon_T^{CO} = 0.24$ eV. Thus, the magnitudes of the two errors are comparable but the signs are opposite. The CO_2 error appears in similar molecules such as HCOOH ($\varepsilon_T^{HCOOH} = -0.19$ eV) and CH_3COOH ($\varepsilon_T^{CH_3COOH} = -0.15$ eV) and is commonly referred to as the OCO backbone error in the literature.[18,19,32,34] Previous studies reported corrections of -0.45 eV for RPBE[19,32] and -0.59 eV for BEEF-vdW,[32] which agree well with our values of -0.46 and -0.56 eV, respectively. The small correction of -0.07 eV for $CO_{(g)}$ in RPBE is likely a reflection of RPBE's original fit against CO adsorption energies.[33] We note in passing that simultaneous OCO/H_2 corrections are also available in the literature for BEEF-vdW of 0.33/0.09,[32] 0.41/0.09,[34] and 0.29/0.10 eV.[18]

We continued the correction procedure, summarized in scheme 4.1, with the simplest molecules in the list, namely, alkanes (only C-H and single C-C bonds) and observed an increasingly positive error depending on the number of hydrocarbon units (-CH_x) (see Table C6). For PBE, that error is on average $\varepsilon_{CH_x} \approx 0.03$ eV/CH_x. Although small, such an error is cumulative, and therefore, for a molecule with 5 -CH_x units it becomes $\varepsilon_{CH_x} \approx 0.03 \frac{\text{eV}}{CH_x} \times 5CH_x \approx 0.15$ eV. Note that we obtained ε_{CH_x} by dividing the error in the formation energy of each alkane by the number of -CH_x units in it and averaging the results for all alkanes in data set A.

Beyond alkanes, one can increase the complexity of the molecules with additional functional groups. For example, we noted that the error for aldehydes and ketones decreased proportionally to the length of the chain. Therefore, to decouple the error associated to carbonyl groups from that of -CH_x groups, we subtracted from the total error of the molecules the error provided by their -CH_x

units (see for instance Table C7). In mathematical terms, for a molecule with the formula $R_1C{=}OR_2$ (where R_1 and R_2 are either -H or -CH_x units): $\varepsilon_T \approx n_C \cdot \varepsilon_{CH_x} + \varepsilon_{-C=O-}$, where n_C is the number of -CH_x units.

To illustrate the use of the formula, consider the total error ($\varepsilon_T^{C_2H_4O}$) for acetaldehyde of -0.09 eV, and the -CH_x error (ε_{CH_x}) of 0.03 eV. The carbonyl-associated error is $\varepsilon_{-C=O-}^{C_2H_4O} \approx \varepsilon_T^{C_2H_4O} - n_C \cdot \varepsilon_{CH_x} = -0.11\,\text{eV}$. Averaging over all the aldehydes and ketones in this study, we obtained $\varepsilon_{-C=O-} = -0.10$ eV for PBE. Table 4.1 shows the CO and CO_2 errors as well as the average errors determined for the following organic functional groups: -C=O- (aldehydes and ketones), -CH_x (alkanes), -(C=O)O- (carboxylic acids and esters) and -OH (alcohols). Note that the error for -(C=O)O- in PBE is identical to that of CO_2, whereas for PW91, RPBE, and BEEF-vdW, that is not the case, as the errors have the same signs but sizably different magnitudes.

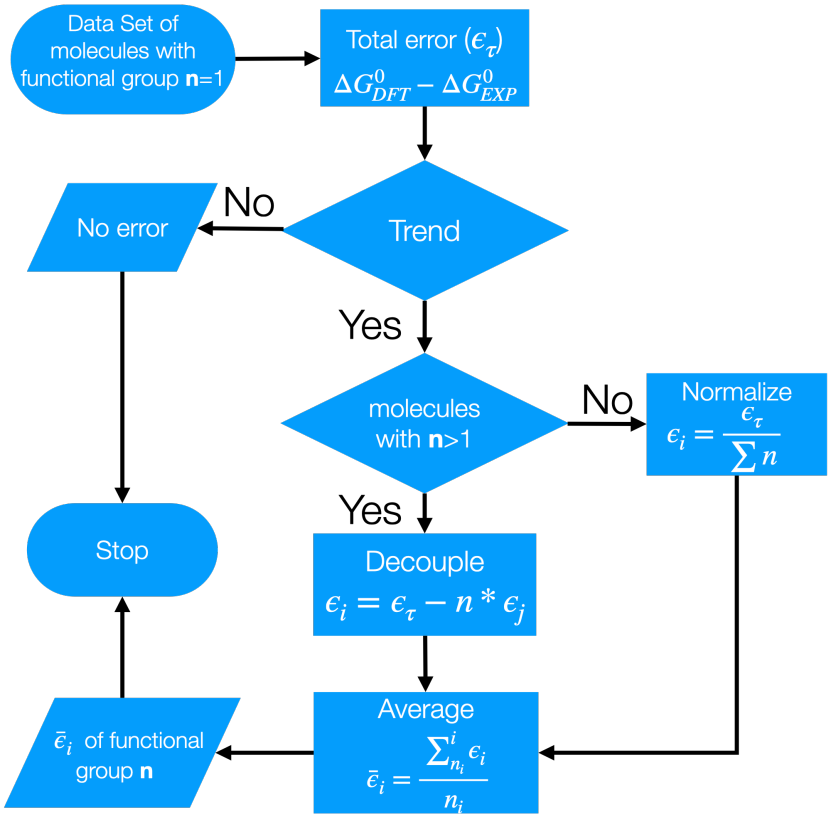

SCHEME 4.1
Workflow to determine functional-dependent errors in energies related to functional groups.

The error in the -OH group for PBE and PW91 is not large enough to warrant correction for simple alcohols. However, this correction may be needed for polyalcohols and in studies focused specifically on methanol and ethanol (see Appendix C, Section C4.1.4 for more details). Before closing this subsection, we stress that a detailed description of the assessment of all errors for every xc-functional can be found in Section C4 in Appendix C. We note that ethylene, acetylene, ethylene oxide and dimethyl ether are present in data set A. Since a larger sample of molecules would be necessary to determine the errors corresponding to their respective functional groups (alkenes, alkynes, and (cyclic) ethers), here the corrections for those molecules are limited to the corrections in the reactants only (CO and CO_2).

TABLE 4.1

Gas-Phase error corrections for the standard free energy of CO_2, CO, and molecules containing -C=O- (Carbonyl Groups in Aldehydes and Ketones), -CHx (Alkanes), and -(C=O)O- (carboxyl groups in carboxylic acids and esters) as per xc functional.[a]

Error	*PBE*	*PW91*	*RPBE*	*BEEF-vdW*
CO_2	-0.19	-0.15	-0.46	-0.56
CO	0.24	0.25	-0.07	-0.18
-C=O-	-0.10	-0.10	-0.21	-0.27
-CHx	0.03	-0.01	0.08	0.21
-(C=O)O-	-0.19	-0.19	-0.27	-0.34 (-0.44)
-OH	-0.04	-0.04	-0.01	-0.14

[a] The two values reported for –(C=O)O– when using BEEF-vdW are for carboxylic acids and esters (the latter in parentheses). All values are in eV.

4.3.2 Implementing Energy Corrections

Data set A was used not only to determine total errors in the formation energies of molecules (ε_T), but also to assess the organic group contributions to such errors (ε_i). In principle, one can use those errors to correct the formation energies of molecules, the combination of which should lead to accurate reaction energies. In this order of ideas, corrected reaction energies ($\Delta G^0_{DFT,\,corr}$) can be calculated as:

$$\Delta G^0_{DFT,\,corr} = \Delta G^0_{DFT} - \left(\sum \varepsilon_T^P - \sum \varepsilon_T^R\right) \qquad 4.6$$

where the sums collect all the errors associated to the reactants (ε_T^R) and products (ε_T^P), taking into account the stoichiometric coefficients. For example, consider the reduction of CO_2 to acetic acid: $2CO_2 + 4H_2 \rightarrow CH_3COOH + 2H_2O$. We find with

RPBE that $\Delta G^0_{DFT} = 0.32$ eV, whereas $\Delta G^0_{\text{exp}} = -0.44$ eV, which corresponds to a large total error $\varepsilon_T^{CH_3COOH} = 0.76$ eV. According to Table 4.1, RPBE has errors associated to the description of CO_2, the -COOH group and the -CH_3 moiety in CH_3COOH. If the errors pinpointed using data set A are contributing to the large total error, suitably correcting CO_2 and CH_3COOH should lead to a sizable reduction of the total error. This is what we find, as $\sum \varepsilon_T^R = 2\varepsilon_T^{CO_2} = -0.92$ eV and $\sum \varepsilon_T^P = \varepsilon_{CH_x} + \varepsilon_{-C=OO-} = -0.19$ eV, so that $\Delta G^0_{DFT,\,corr} = -0.41$ eV, which differs from the experimental value ($\Delta G^0_{\text{exp}} = -0.44$ eV) by 0.03 eV only.

To verify that the errors in the reaction energies of data set B are systematically reduced upon applying the corrections in Table 4.1, we followed a stepwise procedure. First, we applied corrections to data set B only related to reactants (namely CO_2 and CO). Next, we applied corrections related to products. Figure 4.1 and Figure 4.2 show the calculated free energies of reaction versus the experimental free energies for the four functionals studied (PBE, PW91, RPBE, BEEF-vdW). Figure 4.1 provides parity plots for CO-based reactions (Eqs. 4.3 and 4.4) and Figure 4.2 does so for CO_2-based reactions (Eq. 4.5). From the three columns in each figure, the first one corresponds to the non-corrected DFT data, the plots in the second column contain the data upon correcting for reactant-related errors (namely CO or CO_2), and the third column contains the data upon correcting for reactant- and product-related errors altogether.

More molecules can be added to data set A so as to include more organic functional groups and molecules with several groups in their structure. Molecules with alkene, alkyne, epoxy, and ether functional groups as well as aromatic compounds are necessary in data set A to determine their corresponding errors. Here, the free energies of production from CO or CO_2 of ethylene, acetylene, dimethyl ether, and ethylene oxide were corrected for the errors in the reactants only, and no product-related corrections were made (see Table C5).

The gray-shaded areas in Figure 4.1 and Figure 4.2 cover an area around the parity line of ± MAE, and the purple-shaded area extends over ± 0.15 eV around the parity line. For CO reduction reactions and PBE calculations, the MAE is initially 0.61 eV (left column) and is lowered to 0.10 eV after applying the CO correction (central column) and to 0.04 eV after applying both CO and product-related corrections (right column). Similarly, the MAXs go from 1.04 to 0.20 and then to 0.17 eV. For the CO_2 reduction reactions and PBE, the MAE is successively reduced from 0.43 to 0.10 and then to 0.04 eV. Likewise, the MAXs decrease from 1.10 to 0.24 and finally to 0.17 eV. Further details can be found in Table C24, where the MAEs after the first and second correction for all the xc-functionals are provided. We conclude from those values that the errors in data set B are lowered by one order of magnitude once the correction scheme is applied to the species in data set A.

We have included an alternative analysis where data set A is divided into a training set and an extrapolation set in Section C7 of Appendix C. From this analysis we find approximately the same functional-related errors as in Table 4.1 (within ±0.01 eV on average). The MAEs in the extrapolation set after the corrections are comparable to those in Figure 4.1 and Figure 4.2, illustrating the predictive power of the method and its statistical reliability.

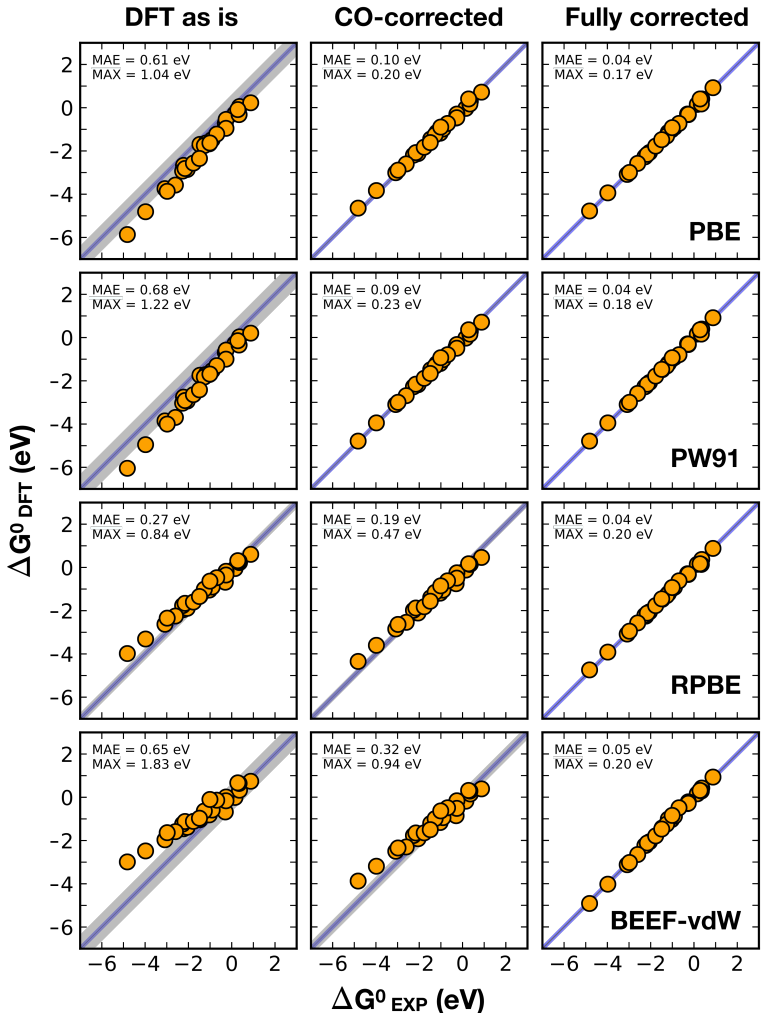

FIGURE 4.1
Parity plots for the experimental and DFT-calculated free energies of production of 27 different compounds from CO and H_2 using PBE, PW91, RPBE and BEEF-vdW. The left column shows the data calculated with DFT without any correction. The center column shows the data upon the first correction (errors in CO), and the right column shows the data after correcting for errors in CO and the products. The mean and maximum absolute errors (MAE and MAX) are shown in each case. The shaded gray area is ± MAE in each case. The blue shaded area around the parity line covers an area of ± 0.15 eV.

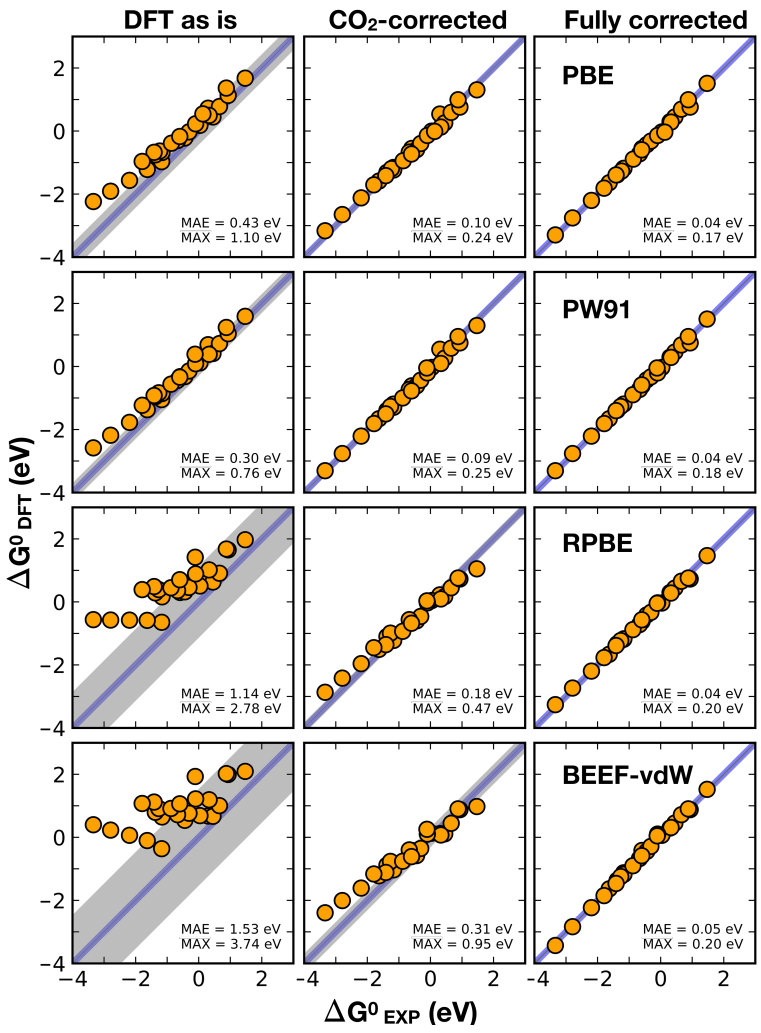

FIGURE 4.2
Parity plot for the experimental and DFT-calculated free energies of production of 27 different products from CO_2 and H_2 using PBE, PW91, RPBE and BEEF-vdW. The left column shows the data calculated with DFT without any correction. The center column shows the data upon the first correction (errors in CO_2), and the right column shows the data after correcting for errors in CO_2 and the products. The mean and maximum absolute errors (MAE and MAX) are shown in each case. The shaded gray area is ± MAE in each case. The blue shaded area around the parity line covers an area of ± 0.15 eV.

4.3.3 Applications in Electrocatalysis

Table 4.2 reveals an important commonality among the xc functionals under study: although the CO and CO_2 errors change from one functional to the next, their difference is nearly constant and equal to ~0.4 eV, on average. This constant energetic separation poses a fundamental limitation for the modeling of catalytic reactions wherein those two compounds are involved, one as a reactant and the other as a product. To show the reaches of this finding, let us consider the example of CO_2 electrocatalytic reduction (CO_2RR) to CO

$$CO_2 + 2\left(H^+ + e^-\right) \rightarrow CO + H_2O_{(l)} \qquad 4.7$$

The backward reaction is known as CO oxidation and is also an important electrocatalytic reaction involved in direct ethanol and methanol fuel cells.[56] Moreover, Eq. 4.7 can also be catalyzed in the gas phase using H_2 in a process called reverse water-gas shift, and the backward reaction is the industrial process known as the water-gas shift.[57] In brief, DFT-based models of this seemingly simple process with numerous applications in electrocatalysis and heterogeneous catalysis may have large gas-phase associated errors.

TABLE 4.2

CO_2 and CO errors and their nearly constant difference ($\varepsilon_T^{CO} - \varepsilon_T^{CO_2}$) across xc-functionals.[a]

Error	*PBE*	*PW91*	*RPBE*	*BEEF-vdW*
CO	0.24	0.25	-0.07	-0.18
CO_2	-0.19	-0.15	-0.46	-0.56
$\varepsilon_T^{CO} - \varepsilon_T^{CO_2}$	0.43	0.40	0.39	0.38
Average	0.40			
Standard deviation	0.02			

[a]All values are in eV.

Figure 4.3 compares CO_2RR to CO on Au(111) single-crystal electrodes using PBE with (Figure 4.3b) and without (Figure 4.3a) gas-phase corrections applied to CO_2 and CO. Likewise, Figures C5 and C6 in Appendix C, section C5, provide data for Au(100) and Au(110). In Figure 4.3a, where DFT data appear as is, the reaction energy of Eq. 4.7 is 0.63 eV. Conversely, it is 0.20 eV in Figure 4.3b, where the energies of CO_2 and CO have been corrected. For comparison, such difference is 0.20 eV in experiments[25] (it is 0.30 eV in Table C3. The difference stems from the liquid state of water in Eq. 4.7). In terms of the equilibrium potential of the reaction, this all means that PBE predicts it to be at -0.32 V vs RHE, whereas both the correction method and experiments set it at -0.10 V vs RHE. The difference is substantial and amounts to ~220 mV. Note in passing that there are no changes in the energy differences between *COOH and *CO, as the corrections are only

applied to the gas phase. Corrections for adsorbates have been proposed before[18] but have escaped the subject and scope of this study.

Within the context of CO_2RR modeling with the computational hydrogen electrode,[47,48] the onset potential is given by the largest-positive consecutive difference in Figure 4.3 ($U_{onset} = -\max(\Delta G_1, \Delta G_2)/e^-$; see the Computational Methods section). In Figure 4.3a, such difference is 0.90 eV, whereas in Figure 4.3b it is 0.71 eV, so that the predicted onset potentials are -0.90 and -0.71 V vs RHE, respectively. As the experimental value of the onset potential is -0.66 V vs RHE,[58] the deviations from experiments are ~0.24 (as is) and 0.05 V (corrected).

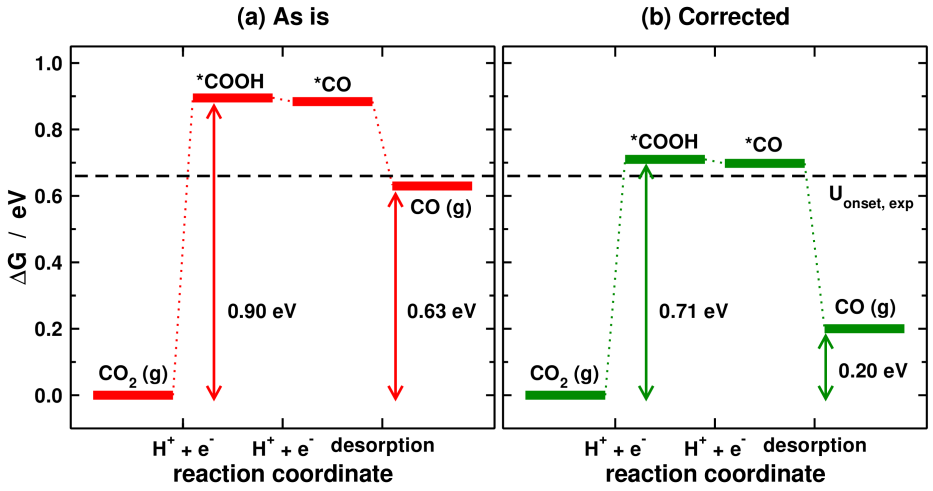

FIGURE 4.3

Free energy diagrams for CO_2 reduction to CO using Au(111) single-crystal electrodes. (a) Using DFT-PBE data as is, and (b) correcting CO_2 and CO for their gas-phase errors. The black dashed line at 0.66 eV marks the free energy corresponding to the experimental onset potential of -0.66 V vs RHE.[58]

We note that the sizable lowering of the error from 0.24 to 0.05 V is a direct result of correcting gas-phase energetics. To assess whether this is a particularity of Au(111) electrodes or part of a more general trend, we also compared the calculated and experimental onset potentials for Au(100), Au(110), Au_{poly}, Ag(111), Ag_{poly}, and Cu_{poly}. The results in Figure 4.4a show that DFT data are systematically deviated from the parity line, which results in a MAE of 0.20 V and a MAX of 0.27 V. Conversely, the CO_2-and-CO corrected data in Figure 4.4b are located around the parity line with MAE = 0.06 V and MAX = 0.09 V. Substantial improvements are also observed for Au(111) and Au(100) using gas-phase corrections with RPBE, see Figures C7-C8. Thus, we conclude that models

for CO_2RR to CO may in general benefit from the gas-phase corrections found in this work.

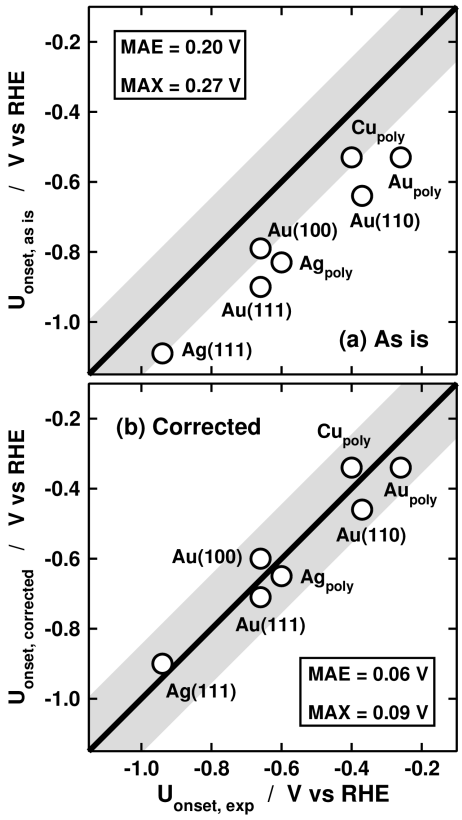

FIGURE 4.4

Parity plots comparing the onset potentials for electrochemical CO_2 reduction to CO using different metals. (a) Using DFT-PBE data as is, and (b) correcting CO_2 and CO for their gas-phase errors. The mean and maximum absolute errors (MAE and MAX) are shown in each case. The gray areas around the parity line cover an area of ± 0.15 V around it. The experimental data were taken from references 58–61 (see details in Table C25).

4.4 Conclusions

When interfaces between metals and fluids are simulated at the GGA level, sizable errors may appear in the description of the gas-phase molecules energetics. Here, we proposed a two-step semiempirical method to determine gas-phase errors, based on the formation energies of 27 different molecules. Furthermore, implementing the corresponding corrections allows for predictions in the analyzed data set of CO_2RR and CORR reaction energies that lower by 1 order of magnitude the average and maximum errors with respect to experiments.

The method also shows that the errors for CO_2 and CO differ by ~0.4 eV for all the examined exchange-correlation functionals. Thus, an intrinsic limitation of DFT exists for the accurate description of reaction energies containing these two molecules, as is the case for CO_2 reduction to CO or HCOOH, CO oxidation to CO_2, etc. Such limited description leads to inaccurate predictions of equilibrium and onset potentials, which may hinder the rational catalyst design.

Conversely, using our correction scheme on various Au, Ag and Cu electrodes decreased the average error in the predicted onset potentials from 0.21 to 0.06 V with respect to experiments. Therefore, in addition to pinpointing and lowering gas-phase errors, the method also helps in providing more accurate electrocatalytic models.

While the present corrections have been applied for electrochemical reactions, the procedure is general enough to be applied to correct the thermochemistry of heterogeneously catalyzed reactions where reactants and products are in the gas phase but the intermediate steps take place at the catalyst surface. Finally, the correction protocol can be enriched by adding more gas-phase molecules to the data set,[62] and using machine learning algorithms to detect and predict errors in structurally more complex substances.

4.5 References

(1) Perdew, J. P. Workhorse Semilocal Density Functional for Condensed Matter Physics and Quantum Chemistry. *Phys. Rev. Lett.* **2009**, *103* (2), 026403.

(2) Cancio, A.; Chen, G. P.; Krull, B. T.; Burke, K. Fitting a Round Peg into a Round Hole: Asymptotically Correcting the Generalized Gradient Approximation for Correlation. *J. Chem. Phys.* **2018**, *149* (8), 084116.

(3) Sun, J.; Ruzsinszky, A.; Perdew, J. P. Strongly Constrained and Appropriately Normed Semilocal Density Functional. *Phys. Rev. Lett.* **2015**, *115* (3), 036402.

(4) Becke, A. D. A New Mixing of Hartree–Fock and Local Density-functional Theories. *J. Chem. Phys.* **1993**, *98* (2), 1372–1377.

(5) Xu, X.; Goddard, W. A. The X3LYP Extended Density Functional for Accurate Descriptions of Nonbond Interactions, Spin States, and Thermochemical Properties. *Proc. Natl. Acad. Sci.* **2004**, *101* (9), 2673–2677.
(6) Maier, T. M.; Arbuznikov, A. V.; Kaupp, M. Local Hybrid Functionals: Theory, Implementation, and Performance of an Emerging New Tool in Quantum Chemistry and Beyond. *Wiley Interdiscip. Rev. Comput. Mol. Sci.* **2019**, *9* (1), e1378.
(7) Dion, M.; Rydberg, H.; Schröder, E.; Langreth, D. C.; Lundqvist, B. I. Van Der Waals Density Functional for General Geometries. *Phys. Rev. Lett.* **2004**, *92* (24), 246401.
(8) Román-Pérez, G.; Soler, J. M. Efficient Implementation of a van Der Waals Density Functional: Application to Double-Wall Carbon Nanotubes. *Phys. Rev. Lett.* **2009**, *103* (9), 096102.
(9) Wellendorff, J.; Lundgaard, K. T.; Møgelhøj, A.; Petzold, V.; Landis, D. D.; Nørskov, J. K.; Bligaard, T.; Jacobsen, K. W. Density Functionals for Surface Science: Exchange-Correlation Model Development with Bayesian Error Estimation. *Phys. Rev. B* **2012**, *85* (23), 235149.
(10) Dudarev, S. L.; Botton, G. A.; Savrasov, S. Y.; Humphreys, C. J.; Sutton, A. P. Electron-Energy-Loss Spectra and the Structural Stability of Nickel Oxide: An LSDA+U Study. *Phys. Rev. B* **1998**, *57* (3), 1505–1509.
(11) Grimme, S.; Antony, J.; Ehrlich, S.; Krieg, H. A Consistent and Accurate Ab Initio Parametrization of Density Functional Dispersion Correction (DFT-D) for the 94 Elements H-Pu. *J. Chem. Phys.* **2010**, *132* (15), 154104.
(12) Caldeweyher, E.; Bannwarth, C.; Grimme, S. Extension of the D3 Dispersion Coefficient Model. *J. Chem. Phys.* **2017**, *147* (3), 034112.
(13) Janthon, P.; Luo, S. (Andy); Kozlov, S. M.; Viñes, F.; Limtrakul, J.; Truhlar, D. G.; Illas, F. Bulk Properties of Transition Metals: A Challenge for the Design of Universal Density Functionals. *J. Chem. Theory Comput.* **2014**, *10* (9), 3832–3839.
(14) Brockherde, F.; Vogt, L.; Li, L.; Tuckerman, M. E.; Burke, K.; Müller, K.-R. Bypassing the Kohn-Sham Equations with Machine Learning. *Nat. Commun.* **2017**, *8* (1), 1–10.
(15) Lejaeghere, K.; Bihlmayer, G.; Björkman, T.; Blaha, P.; Blügel, S.; Blum, V.; Caliste, D.; Castelli, I. E.; Clark, S. J.; Corso, A. D.; Gironcoli, S. de; Deutsch, T.; Dewhurst, J. K.; Marco, I. D.; Draxl, C.; Dułak, M.; Eriksson, O.; Flores-Livas, J. A.; Garrity, K. F.; Genovese, L.; Giannozzi, P.; Giantomassi, M.; Goedecker, S.; Gonze, X.; Grånäs, O.; Gross, E. K. U.; Gulans, A.; Gygi, F.; Hamann, D. R.; Hasnip, P. J.; Holzwarth, N. a. W.; Iuşan, D.; Jochym, D. B.; Jollet, F.; Jones, D.; Kresse, G.; Koepernik, K.; Küçükbenli, E.; Kvashnin, Y. O.; Locht, I. L. M.; Lubeck, S.; Marsman, M.; Marzari, N.; Nitzsche, U.; Nordström, L.; Ozaki, T.; Paulatto, L.; Pickard, C. J.; Poelmans, W.; Probert, M. I. J.; Refson, K.; Richter, M.; Rignanese, G.-M.; Saha, S.; Scheffler, M.; Schlipf, M.; Schwarz, K.; Sharma, S.; Tavazza, F.; Thunström, P.; Tkatchenko, A.; Torrent, M.; Vanderbilt, D.; Setten, M. J. van; Speybroeck, V. V.; Wills, J. M.; Yates, J. R.; Zhang, G.-X.; Cottenier, S. Reproducibility in Density Functional Theory Calculations of Solids. *Science* **2016**, *351* (6280), aad3000.

(16) Kurth, S.; Perdew, J. P.; Blaha, P. Molecular and Solid-State Tests of Density Functional Approximations: LSD, GGAs, and Meta-GGAs. *Int. J. Quantum Chem.* **1999**, *75* (4–5), 889–909.

(17) Briquet, L. G. V.; Sarwar, M.; Mugo, J.; Jones, G.; Calle-Vallejo, F. A New Type of Scaling Relations to Assess the Accuracy of Computational Predictions of Catalytic Activities Applied to the Oxygen Evolution Reaction. *ChemCatChem* **2017**, *9* (7), 1261–1268.

(18) Christensen, R.; Hansen, H. A.; Vegge, T. Identifying Systematic DFT Errors in Catalytic Reactions. *Catal. Sci. Technol.* **2015**, *5* (11), 4946–4949.

(19) Peterson, A. A.; Abild-Pedersen, F.; Studt, F.; Rossmeisl, J.; Nørskov, J. K. How Copper Catalyzes the Electroreduction of Carbon Dioxide into Hydrocarbon Fuels. *Energy Environ. Sci.* **2010**, *3* (9), 1311–1315.

(20) Calle-Vallejo, F.; Martínez, J. I.; García-Lastra, J. M.; Mogensen, M.; Rossmeisl, J. Trends in Stability of Perovskite Oxides. *Angew. Chem. Int. Ed.* **2010**, *49* (42), 7699–7701.

(21) Bartel, C. J.; Weimer, A. W.; Lany, S.; Musgrave, C. B.; Holder, A. M. The Role of Decomposition Reactions in Assessing First-Principles Predictions of Solid Stability. *Npj Comput. Mater.* **2019**, *5* (1), 1–9.

(22) Tameh, M. S.; Dearden, A. K.; Huang, C. Accuracy of Density Functional Theory for Predicting Kinetics of Methanol Synthesis from CO and CO2 Hydrogenation on Copper. *J. Phys. Chem. C* **2018**, *122* (31), 17942–17953.

(23) Blaylock, D. W.; Ogura, T.; Green, W. H.; Beran, G. J. O. Computational Investigation of Thermochemistry and Kinetics of Steam Methane Reforming on Ni(111) under Realistic Conditions. *J. Phys. Chem. C* **2009**, *113* (12), 4898–4908.

(24) Bushuyev, O. S.; Luna, P. D.; Dinh, C. T.; Tao, L.; Saur, G.; Lagemaat, J. van de; Kelley, S. O.; Sargent, E. H. What Should We Make with CO2 and How Can We Make It? *Joule* **2018**, *2* (5), 825–832.

(25) Nitopi, S.; Bertheussen, E.; Scott, S. B.; Liu, X.; Engstfeld, A. K.; Horch, S.; Seger, B.; Stephens, I. E. L.; Chan, K.; Hahn, C.; Nørskov, J. K.; Jaramillo, T. F.; Chorkendorff, I. Progress and Perspectives of Electrochemical CO2 Reduction on Copper in Aqueous Electrolyte. *Chem. Rev.* **2019**, *119* (12), 7610–7672.

(26) Birdja, Y. Y.; Pérez-Gallent, E.; Figueiredo, M. C.; Göttle, A. J.; Calle-Vallejo, F.; Koper, M. T. M. Advances and Challenges in Understanding the Electrocatalytic Conversion of Carbon Dioxide to Fuels. *Nat. Energy* **2019**, *4* (9), 732–745.

(27) Calle-Vallejo, F.; Tymoczko, J.; Colic, V.; Vu, Q. H.; Pohl, M. D.; Morgenstern, K.; Loffreda, D.; Sautet, P.; Schuhmann, W.; Bandarenka, A. S. Finding Optimal Surface Sites on Heterogeneous Catalysts by Counting Nearest Neighbors. *Science* **2015**, *350* (6257), 185–189.

(28) Seh, Z. W.; Kibsgaard, J.; Dickens, C. F.; Chorkendorff, I.; Nørskov, J. K.; Jaramillo, T. F. Combining Theory and Experiment in Electrocatalysis: Insights into Materials Design. *Science* **2017**, *355* (6321), eaad4998.

(29) Garlyyev, B.; Fichtner, J.; Piqué, O.; Schneider, O.; Bandarenka, A. S.; Calle-Vallejo, F. Revealing the Nature of Active Sites in Electrocatalysis. *Chem. Sci.* **2019**, *10* (35), 8060–8075.
(30) Jovanov, Z. P.; Hansen, H. A.; Varela, A. S.; Malacrida, P.; Peterson, A. A.; Nørskov, J. K.; Stephens, I. E. L.; Chorkendorff, I. Opportunities and Challenges in the Electrocatalysis of CO2 and CO Reduction Using Bifunctional Surfaces: A Theoretical and Experimental Study of Au–Cd Alloys. *J. Catal.* **2016**, *343*, 215–231.
(31) Kresse, G.; Furthmüller, J. Efficient Iterative Schemes for Ab Initio Total-Energy Calculations Using a Plane-Wave Basis Set. *Phys. Rev. B* **1996**, *54* (16), 11169–11186.
(32) Studt, F.; Abild-Pedersen, F.; Varley, J. B.; Nørskov, J. K. CO and CO2 Hydrogenation to Methanol Calculated Using the BEEF-VdW Functional. *Catal. Lett.* **2013**, *143* (1), 71–73.
(33) Hammer, B.; Hansen, L. B.; Nørskov, J. K. Improved Adsorption Energetics within Density-Functional Theory Using Revised Perdew-Burke-Ernzerhof Functionals. *Phys. Rev. B* **1999**, *59* (11), 7413–7421.
(34) Studt, F.; Behrens, M.; Kunkes, E. L.; Thomas, N.; Zander, S.; Tarasov, A.; Schumann, J.; Frei, E.; Varley, J. B.; Abild-Pedersen, F.; Nørskov, J. K.; Schlögl, R. The Mechanism of CO and CO2 Hydrogenation to Methanol over Cu-Based Catalysts. *ChemCatChem* **2015**, *7* (7), 1105–1111.
(35) Perdew, J. P.; Burke, K.; Ernzerhof, M. Generalized Gradient Approximation Made Simple. *Phys. Rev. Lett.* **1996**, *77* (18), 3865–3868.
(36) Perdew, J. P.; Burke, K.; Wang, Y. Generalized Gradient Approximation for the Exchange-Correlation Hole of a Many-Electron System. *Phys. Rev. B* **1996**, *54* (23), 16533–16539.
(37) Kresse, G.; Joubert, D. From Ultrasoft Pseudopotentials to the Projector Augmented-Wave Method. *Phys. Rev. B* **1999**, *59* (3), 1758–1775.
(38) Wang, W.; Dai, S.; Li, X.; Yang, J.; Srolovitz, D. J.; Zheng, Q. Measurement of the Cleavage Energy of Graphite. *Nat. Commun.* **2015**, *6* (1), 1–7.
(39) Girifalco, L. A.; Lad, R. A. Energy of Cohesion, Compressibility, and the Potential Energy Functions of the Graphite System. *J. Chem. Phys.* **1956**, *25* (4), 693–697.
(40) Zacharia, R.; Ulbricht, H.; Hertel, T. Interlayer Cohesive Energy of Graphite from Thermal Desorption of Polyaromatic Hydrocarbons. *Phys. Rev. B* **2004**, *69* (15), 155406.
(41) Benedict, L. X.; Chopra, N. G.; Cohen, M. L.; Zettl, A.; Louie, S. G.; Crespi, V. H. Microscopic Determination of the Interlayer Binding Energy in Graphite. *Chem. Phys. Lett.* **1998**, *286* (5), 490–496.
(42) Xia, M.; Liang, C.; Cheng, Z.; Hu, R.; Liu, S. The Adhesion Energy Measured by a Stress Accumulation-Peeling Mechanism in the Exfoliation of Graphite. *Phys. Chem. Chem. Phys.* **2019**, *21* (3), 1217–1223.
(43) Liu, Z.; Liu, J. Z.; Cheng, Y.; Li, Z.; Wang, L.; Zheng, Q. Interlayer Binding Energy of Graphite: A Mesoscopic Determination from Deformation. *Phys. Rev. B* **2012**, *85* (20), 205418.

(44) Lide, D. R. CRC Handbook of Chemistry and Physics, 85th Edition; CRC Press, 2004.
(45) Chase, Jr., M. W.; Davies, C. A.; Downey, Jr., J. R.; Frurip, D. J.; MacDonald, R. A.; Syverud, A. N. NIST-JANAF Thermochemical Tables. *J. Phys. Chem. Ref. Data* **1985**, *Suppl. 1 to Vol. 14*, 1856.
(46) Informatics, N. O. of D. and. NIST Chemistry WebBook https://webbook.nist.gov/chemistry/ (accessed Oct 18, 2019).
(47) Hansen, H. A.; Varley, J. B.; Peterson, A. A.; Nørskov, J. K. Understanding Trends in the Electrocatalytic Activity of Metals and Enzymes for CO2 Reduction to CO. *J. Phys. Chem. Lett.* **2013**, *4* (3), 388–392.
(48) Nørskov, J. K.; Rossmeisl, J.; Logadottir, A.; Lindqvist, L.; Kitchin, J. R.; Bligaard, T.; Jónsson, H. Origin of the Overpotential for Oxygen Reduction at a Fuel-Cell Cathode. *J. Phys. Chem. B* **2004**, *108* (46), 17886–17892.
(49) Akhade, S. A.; McCrum, I. T.; Janik, M. J. The Impact of Specifically Adsorbed Ions on the Copper-Catalyzed Electroreduction of CO2. *J. Electrochem. Soc.* **2016**, *163* (6), F477.
(50) Pérez-Gallent, E.; Marcandalli, G.; Figueiredo, M. C.; Calle-Vallejo, F.; Koper, M. T. M. Structure- and Potential-Dependent Cation Effects on CO Reduction at Copper Single-Crystal Electrodes. *J. Am. Chem. Soc.* **2017**, *139* (45), 16412–16419.
(51) Ringe, S.; Clark, E. L.; Resasco, J.; Walton, A.; Seger, B.; Bell, A. T.; Chan, K. Understanding Cation Effects in Electrochemical CO2 Reduction. *Energy Environ. Sci.* **2019**, *12* (10), 3001–3014.
(52) Singh, M. R.; Kwon, Y.; Lum, Y.; Ager, J. W.; Bell, A. T. Hydrolysis of Electrolyte Cations Enhances the Electrochemical Reduction of CO2 over Ag and Cu. *J. Am. Chem. Soc.* **2016**, *138* (39), 13006–13012.
(53) Resasco, J.; Chen, L. D.; Clark, E.; Tsai, C.; Hahn, C.; Jaramillo, T. F.; Chan, K.; Bell, A. T. Promoter Effects of Alkali Metal Cations on the Electrochemical Reduction of Carbon Dioxide. *J. Am. Chem. Soc.* **2017**, *139* (32), 11277–11287.
(54) Benson, S. W.; Buss, J. H. Additivity Rules for the Estimation of Molecular Properties. Thermodynamic Properties. *J. Chem. Phys.* **1958**, *29* (3), 546–572.
(55) Teng, B.-T.; Wen, X.-D.; Fan, M.; Wu, F.-M.; Zhang, Y. Choosing a Proper Exchange–Correlation Functional for the Computational Catalysis on Surface. *Phys. Chem. Chem. Phys.* **2014**, *16* (34), 18563–18569.
(56) Lamy, C.; Lima, A.; LeRhun, V.; Delime, F.; Coutanceau, C.; Léger, J.-M. Recent Advances in the Development of Direct Alcohol Fuel Cells (DAFC). *J. Power Sources* **2002**, *105* (2), 283–296.
(57) Ratnasamy, C.; Wagner, J. P. Water Gas Shift Catalysis. *Catal. Rev.* **2009**, *51* (3), 325–440.
(58) Todoroki, N.; Tei, H.; Tsurumaki, H.; Miyakawa, T.; Inoue, T.; Wadayama, T. Surface Atomic Arrangement Dependence of Electrochemical CO2 Reduction on Gold: Online Electrochemical Mass Spectrometric Study on Low-Index Au(Hkl) Surfaces. *ACS Catal.* **2019**, *9* (2), 1383–1388.
(59) Kuhl, K. P.; Hatsukade, T.; Cave, E. R.; Abram, D. N.; Kibsgaard, J.; Jaramillo, T. F. Electrocatalytic Conversion of Carbon Dioxide to Methane and Methanol on Transition Metal Surfaces. *J. Am. Chem. Soc.* **2014**, *136* (40), 14107–14113.

(60) Hoshi, N.; Kato, M.; Hori, Y. Electrochemical Reduction of CO2 on Single Crystal Electrodes of Silver Ag(111), Ag(100) and Ag(110). *J. Electroanal. Chem.* **1997**, *440* (1), 283–286.

(61) Ma, M.; Trześniewski, B. J.; Xie, J.; Smith, W. A. Selective and Efficient Reduction of Carbon Dioxide to Carbon Monoxide on Oxide-Derived Nanostructured Silver Electrocatalysts. *Angew. Chem. Int. Ed.* **2016**, *55* (33), 9748–9752.

(62) Urrego-Ortiz, R.; Builes, S.; Calle-Vallejo, F. Fast Correction of Errors in the DFT-Calculated Energies of Gaseous Nitrogen-Containing Species. *ChemCatChem* **2021**. doi.org/10.1002/cctc.202100125